Tracking the Recruitment of Diabetogenic CD8$^+$ T-Cells to the Pancreas in Real Time

Anna Moore,[1] Jan Grimm,[2] Bingye Han,[3] and Pere Santamaria[3]

Development of autoimmune diabetes in both humans and mice is preceded by a prolonged period of inflammation of pancreatic islets by autoreactive T-cells. Noninvasive imaging techniques, including positron-emission tomography and optical or magnetic resonance imaging, have been used to track the recruitment of lymphocytes to sites of inflammation. These techniques, however, rely on labeling strategies that are non–antigen specific and do not allow specific tracking of the recruitment of autoreactive lymphocytes. Here we describe an antigen-specific magnetic label to selectively target a prevalent population of diabetogenic CD8$^+$ T-cells that contribute to the progression of insulitis to overt diabetes in NOD mice. Superparamagnetic nanoparticles coated with multiple copies of a high-avidity peptide/major histocompatibility complex ligand of these T-cells (NRP-V7/K^d) are endocytosed by CD8$^+$ T-cells in an antigen-specific manner. Using these T-cells as probes, we show that inflammation of pancreatic islets by autoreactive T-cells can be detected in real time by magnetic resonance imaging. This study demonstrates the feasibility of visualizing the presence of ongoing autoimmune responses noninvasively. *Diabetes* 53:1459–1466, 2004

In vivo tracking of autoreactive lymphocytes in intact micro- and macroenvironments in real time has been a long-sought goal of imaging techniques in the context of autoimmunity. Type 1 diabetes is an organ-specific autoimmune disease that results from destruction of pancreatic β-cells by autoreactive CD4$^+$ and CD8$^+$ T-cells. Development of clinical symptoms of diabetes is preceded by a prolonged period of mononuclear cell infiltration of pancreatic islets that involves the recruitment and differentiation of autoreactive T-cells into cytolytic effectors (1). The recent introduction of small animal imaging systems has made it possible to track T-cells and other immune cells in deep organs in rodents (2). In particular, positron-emission tomography imaging of radiolabeled cells (3–7) and bioluminescence imaging of cells expressing luciferase (8–12) have been used to image cell trafficking in small animals. Although sensitive, these techniques lack high spatial resolution. Although intravital microscopy provides greater spatial resolution (13), it involves invasive procedures.

Magnetic resonance imaging (MRI) is a noninvasive approach that offers high spatial resolution in vivo. Cells labeled with superparamagnetic monocrystalline iron oxide nanoparticles and their derivatives (14,15) can be visualized at the single-cell level (10–100 μm voxel resolution) using high-resolution MRI (16–18). However, a fundamental limitation of this and other labeling techniques in the context of autoimmunity is that they are not cell specific and do not allow discrimination between autoreactive and irrelevant lymphocyte specificities. Thus, the goal of this study was to engineer a new generation of magnetic imaging probes that are capable of labeling specific populations of autoreactive lymphocytes within the total lymphocyte pool of a given individual. These T-cells then could be tracked to sites of ongoing inflammation in vivo using MRI.

We and others have proposed that the initial β-cell insult that triggers the shedding of β-cell autoantigens and their loading onto dendritic cells and the activation of autoreactive CD4$^+$ T-cells in spontaneous autoimmune diabetes in NOD mice is effected by CD8$^+$ cytotoxic T-cells (19–22). Although the nature of the CD8$^+$ T-cell subpopulation that contributes to the initiation of autoimmune diabetes remains to be determined, several lines of evidence suggest that this subpopulation is dominated by clonotypes expressing Vα17-Jα42 T-cell receptor α (TCR-α) chains. These clonotypes are K^d-restricted, recognize the same peptide ligands (NOD-relevant V7 peptide [NRP-V7] and some of its mimics [23,24]), are present at a very high frequency in the peripheral blood of young NOD mice (25), and constitute a large fraction of the CD8$^+$ cells that can be propagated from the earliest insulitic lesions of NOD mice (22). Moreover, they are highly diabetogenic in TCR-transgenic mice (20,21) and undergo an avidity maturation process that contributes to the progression of insulitis to overt disease in wild-type NOD mice (26). The existence of such a prevalent, highly diabetogenic population of autoreactive lymphocytes thus affords the unique opportunity to test the usefulness of MRI to visualize the progressive accumulation of autoreactive T-cells to the corresponding target organ, the pancreas.

From the [1]Athinoula A. Martinos Center for Biomedical Imaging, Department of Radiology, Massachusetts General Hospital, Charlestown, Massachusetts; the [2]Center for Molecular Imaging Research, Department of Radiology, Massachusetts General Hospital and Harvard Medical School, Boston, Massachusetts; and the [3]Julia McFarlane Diabetes Research Center and Department of Microbiology and Infectious Diseases, University of Calgary, Alberta, Canada.

Address correspondence and reprint requests to Anna Moore, PhD, MGH/MIT/HMS Athinoula A. Martinos Center for Biomedical Imaging, Department of Radiology, Massachusetts General Hospital, Building 149, 13th Street, Room 2301, Charlestown, MA 02129. E-mail: amoore@helix.mgh.harvard.edu.

Received for publication 1 December 2003 and accepted in revised form 8 March 2004.

FACS, fluorescence-activated cell sorter; FITC, fluorescein isothiocyanate; H&E, hematoxylin and eosin; IGRP, islet-specific glucose-6-phosphatase catalytic subunit–related protein; MHC, major histocompatibility complex; MRI, magnetic resonance imaging; PE, phycoerythrin; SI, signal intensity; TCR, T-cell receptor.

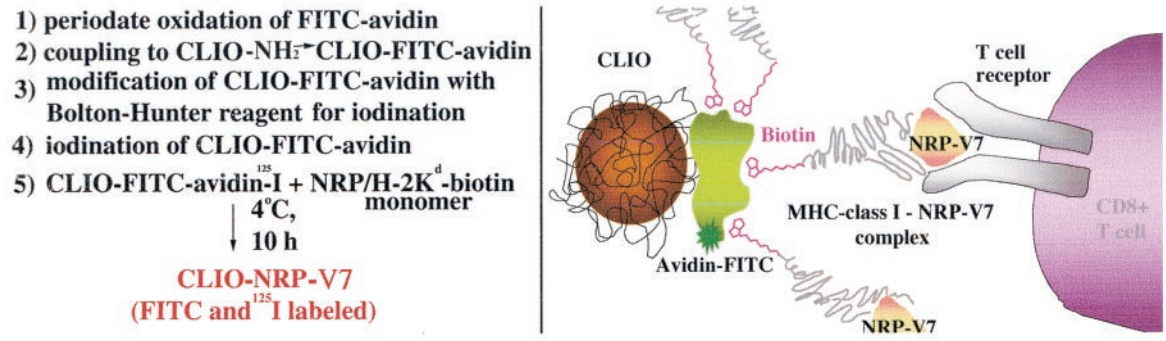

FIG. 1. ***Left*****: Step-by-step synthesis of CLIO-NRP-V7 probe.** ***Right*****: Schematic representation of CLIO-NRP-V7 probe. Biotinylated NRP-V7/H-2K^d complex was coupled to CLIO particles modified with avidin. CLIO-NRP-V7 probe is recognized by the TCR on NRP-V7–reactive CD8$^+$ T-cells. Note that there are four binding sites for biotin on avidin and, hence, for biotinylated peptide/MHC complex.**

Here we have developed a magnetic imaging probe that exclusively labels this subset of NRP-V7–reactive CD8$^+$ T-cells. Importantly, we show that progressive accumulation of these T-cells in the pancreas of live mice can be visualized in real time using high-resolution MRI. This imaging technique, involving the selective labeling of prevalent subpopulations of diabetogenic lymphocytes within the circulating lymphocyte pool, may one day be suitable for detection of islet inflammation in predisposed individuals or for the prediction of recurrent disease after pancreas or islet transplantation. In addition, it may aid in investigating the precise mechanisms involved in the initiation and progression of β-cell destruction by autoreactive T-cells.

RESEARCH DESIGN AND METHODS

Synthesis of CLIO-NRP-V7 nanoparticle. A dextran-coated superparamagnetic iron oxide nanoparticle was synthesized, cross-linked with epichlorohydrin, and treated with ammonia to produce amino-CLIO (CLIO-NH_2) (27). Amino-CLIO (0.2 mmol of Fe) and fluorescein-labeled hen egg white avidin (7.5×10^{-5} mmol; Pierce, Rockford, IL) were dialyzed separately against 0.01 mol/l sodium acetate buffer (pH 6.0) for 2 h. Sodium periodate (46 μmol) was added to the avidin, incubated for 30 min at room temperature in the dark, and dialyzed against 150 mmol/l sodium chloride. The oxidized avidin was added to amino-CLIO, and the pH was adjusted by the addition of 100 μl of 0.2 mol/l sodium bicarbonate (pH 9.5). The mixture was incubated for 2.5 h under stirring. Sodium cyanoborohydride was then added (80 μmol), and the mixture was incubated for 3.5 h at room temperature to reduce Schiff's base and produce stable covalent bond. The CLIO-avidin nanoparticles were separated from unreacted avidin using a magnetic separation column (Miltenyi Biotec, Auburn, CA). Iron was determined spectrophotometrically, and protein was determined by the BCA method (Pierce). The number of avidin molecules per nanoparticle was obtained from concentrations of avidin and iron, assuming 2,064 iron atoms per particle (28). Biotinylated NRP-V7/H-2K^d or irrelevant TUM/H-2K^d monomer (24) was added at a molar ratio of 4 mol biotin/mol avidin. Biotinylated proteins were added in multiple portions (~0.4 mol biotin/avidin) over a period of 24 h at 4°C with slow stirring (10 rpm). CLIO-NRP-V7 was purified on a magnetic separation column.

For performing cell internalization studies before conjugation to the monomer, avidin-CLIO was also iodinated. Because of a lack of accessible tyrosines on avidin, avidin-CLIO was reacted with Bolton-Hunter reagent to introduce a 3-(4-hydroxyphenyl) propionyl group. Iodination was performed using the Iodogen method (Pierce). The nanoparticle denoted CLIO-NRP-V7 is depicted in Fig. 1. CLIO-NRP-V7 thus contains fluorescein isothiocyanate (FITC) for fluorescence-activated cell sorter (FACS) analysis, ^{125}I on the avidin to quantitate cell uptake, and a superparamagnetic iron oxide core for MRI.

Characterization of CLIO-NRP-V7 nanoparticles. Nanoparticle size was determined by light scattering (submicron particle size analyzer, Coulter N-4; Coulter, Hialeah, FL), and relaxivity (change in relaxation rate per mmol) was measured at 0.47 T (20 MHz) and 37°C using a Bruker NMS-120 MR spectrometer. The number of biotin binding sites on avidin-CLIO was determined by incubating 60×10^{-4} μmol/l of ^{3}H-biotin (NEN Life Science Products, Boston, MA) with 6×10^{-4} μmol/l of CLIO-avidin for 24 h at 4°C. CLIO-avidin was separated from free biotin using a PD-10 column equilibrated with PBS and eluted in the same buffer. Fractions were counted (Tri-Carb 1900CA; Packard, Downers Grove, IL) and analyzed for iron content. The number of biotin binding sites per avidin was calculated using the biotin specific activity provided by the manufacturer (51.1 Ci · mmol^{-1} · l^{-1}).

For assessing the ability of the CLIO-avidin to react with high molecular biotinylated proteins, CLIO-avidin was reacted with biotinylated BSA. This reaction was monitored by changes in the spin-spin relaxation time T2, which was used as a measure of particle aggregation into clusters. Biotinylated BSA induces the dispersed avidin-CLIO to form nanoparticle clusters, which have a higher relaxivity than the dispersed state (29). For effecting a switch from dispersed to clustered nanoparticles, CLIO-avidin or amino-CLIO was mixed with BSA-biotin so that a ratio of 4 mol biotin/mol avidin was achieved. Compounds were reacted for 24 h at 4°C with slow stirring. Relaxation time measurements were performed as described above.

Specificity of CLIO-NRP-V7 for NRP-V7–reactive CD8$^+$ T-cells. The interaction of CLIO-NRP-V7 with CD8$^+$ T-cells was determined using cells from 8.3-NOD mice, which express a transgenic NRP-V7–reactive TCR (21). Control CD8$^+$ T-cells were obtained from pre-diabetic nontransgenic NOD mice. Splenic CD8$^+$ T-cells were purified by high-affinity negative selection according to the manufacturer's instructions (R&D Systems, Minneapolis, MN). Purity of CD8$^+$ T-cells was assessed by FACS analysis (FACScan; Becton Dickinson Immunocytometry Systems, Mountain View, CA) with FITC or phycoerythrin (PE)-labeled anti-CD8 and anti-CD3 antibodies (Pharmingen, San Diego, CA).

For FACS analysis, CD8$^+$ T-cells from nondiabetic 8.3-NOD mice and from wild-type NOD mice were incubated with CLIO-NRP-V7 (50 μg Fe) for 1 h and washed. After a final centrifugation, cells were fixed in 2% paraformaldehyde and subjected to FACS analysis. For assessing whether intravital labeling of CD8$^+$ T-cells occurs as well in vivo, 8.3-NOD mice and pre-diabetic NOD mice received an injection of CLIO-NRP-V7 (10 mg Fe/kg). Twenty-four hours later, blood was withdrawn via cardiac puncture and subjected to FACS analysis after erythrocyte lysis and labeling the rest of the cell pool with PE-labeled anti-CD8 antibodies.

For calculating the amount of iron associated with the cells, CD8$^+$ T-cells from 8.3-NOD mice were incubated with various amounts (1–50 μg Fe) of iodinated CLIO-NRP-V7 as described above, followed by extensive washing with Hanks' balanced salt solution underlaid with 1 ml of 40% Histopaque-1077. After final centrifugation and aspiration of the supernatant, cell pellets were counted in a γ-counter (1289 Compugamma LS; Wallac, Turku, Finland). Control experiments included incubation of the cells with the same amounts of CLIO-avidin or CLIO-TUM. All experiments were performed in triplicate.

Fluorescence microscopy and histology of frozen sections. Frozen sections of pancreata from nondiabetic 8.3-NOD mice were fixed in cold acetone for 2 min at −20°C and incubated with the CLIO-NRP-V7 probe followed by 1 h of incubation with anti–CD8-PE antibodies diluted 1:50 in PBS with 10% horse serum (Pharmingen) and subjected to dual-channel fluorescence microscopy (Zeiss Axiovert 100TV; Carl Zeiss, Wetzlar, Germany). Images were collected using a cooled charged-coupled device (Photometrics, Tucson, AZ) with appropriate excitation and emission filters (Omega Optical, Brattleboro, VT).

After MRI, pancreata were excised, snap frozen, and sliced into 7-μm sections. Sections were incubated with anti–CD8-PE antibodies and subjected

to dual-channel fluorescence microscopy as described above. Consecutive sections were stained with hematoxylin and eosin (H&E).

Cytokine secretion and ^{51}Cr-release assay. To determine whether probe labeling altered the ability of the T-cells to secrete cytokines in response to antigen stimulation, we challenged labeled and unlabeled cells with NRP-V7-peptide–pulsed splenocytes. $CD8^+$ T-cells (2×10^4 cells/well) were labeled with CLIO-NRP-V7 and incubated with NRP-V7–pulsed irradiated NOD splenocytes for 48 h at 37°C, and the supernatants were assayed for interleukin-2 and interferon-γ using enzyme-linked immunosorbent assay kits (Genzyme, Cambridge, MA) as described previously (23).

RMA-SK^d cells (preincubated at 26°C overnight [30]) were labeled with [^{51}Cr]sodium chromate (DuPont-NEN, Boston, MA) for 2 h, washed, resuspended at 10^5 cells/ml in RPMI 1640 containing 0.25% BSA, seeded at 10^4 cells · 100 μl^{-1} · well^{-1}, pulsed with NRP-V7 peptide (1 μmol/l) for 1 h at 37°C, and used as target cells in a ^{51}Cr-release assay. Effectors (8.3-$CD8^+$ T-cells) were added to each well at different target/effector ratios. Cultures that contained peptide but not T-cells were used as controls. The plates were incubated at 37°C for 8 h, and the supernatants were collected for determination of ^{51}Cr release. Results were expressed as specific lysis (in %) = 100 × (test cpm − spontaneous cpm)/(total cpm − spontaneous cpm) taking into account spontaneous ^{51}Cr release and total ^{51}Cr release in the presence of 5% Triton X-100 with appropriate controls. Toxicity of the probe toward $CD8^+$ T-cells was tested in cytotoxicity assays (CytoTox 96; Promega, Madison, WI).

In vivo MRI. To investigate whether homing of labeled autoreactive $CD8^+$ T-cells could be visualized in the mouse pancreas in vivo, we performed in vivo MRI experiments. For these studies, $CD8^+$ T-cells harvested from 8.3-NOD mice were labeled with CLIO-NRP-V7 as described above. After the final wash, 2×10^7 labeled cells were transferred intraperitoneally into 5-week-old NOD.scid mice ($n = 5$). MRI was performed on anesthetized animals before and 1, 3, 4, 5, 9, 13, and 16 days after cell transfer. MRI was performed using a superconducting magnet (NMR Magnex Scientific, Concord, CA), equipped with Numaris 5.0 Software (Siemens, Erlangen, Germany) and a custom-made 3-in surface coil (MRI Imaging Center, Massachusetts General Hospital, Charlestown, MA). The imaging protocol consisted of coronal T1 weighted spin echo and T2-weighted turbo spin echo pulse sequences. The standard T1 weighted sequence had the following parameters: spin echo 600/13 (TR/TE), three acquisitions, 30 slices with a slice thickness of 0.5 mm, field of view 53 × 53 mm, matrix 512 × 512, resulting in a voxel size of 103 × 103 × 500 μm. The parameters for the T2-weighted sequence were the following: turbo spin echo 3,000/29 (TR/TE), two acquisitions, echo spacing 12.5 ms. Twenty slices with a slice thickness of 0.5 mm, field of view of 60 × 36 mm, and matrix of 512 × 512 were acquired, resulting in a voxel size of 120 × 72 × 500 μm. Ten minutes before imaging, mice received an intraperitoneal injection of scopolamine butylbromide (Buscopan, 0.5 mg/kg; Boehringer, Ingelheim, Germany) to reduce peristaltic motion of bowel. Image analysis was performed using Image J 1.26T software (National Institutes of Health, Bethesda, MD). Regions of interest were drawn around the tail of the pancreas, and signal intensity (SI) was compared with that in an external control (1 mmol/l standard solution of $GdCl_3$). Statistical analysis was performed using InStat 2.03 software (GraphPad Software, San Diego, CA). Blood glucose level was measured from tail snip in fed state at 10:00 A.M. daily using the Glucometer Elite XL (Bayer, Eikhart, IN).

All experiments including animals were performed in compliance with institutional guidelines and according to the protocols approved by the Subcommittee on Research Animals Care at Massachusetts General Hospital.

RESULTS

Synthesis and characterization of an antigen-based $CD8^+$ T-cell–specific magnetic probe. To synthesize a magnetic probe that is capable of specifically labeling NRP-V7–reactive $CD8^+$ T-cells, we first modified aminated cross-linked iron oxide nanoparticles (27) with FITC-labeled avidin using periodate oxidation. The resultant compound (CLIO-avidin) contained on average between one and two avidin molecules per CLIO particle. We then coupled CLIO-avidin with a biotinylated monomeric major histocompatibility complex (MHC) class I peptide complex carrying NRP-V7 (NRP-V7/H-2K^d; Fig. 1). Avidin-biotin formation, which does not require any chemical modification of the monomer, was used to preserve the immunologic properties of the monomers. The number of binding sites for biotin calculated from the binding reaction with ^{3}H-biotin was 3.8 mol of biotin per mole of avidin in CLIO-avidin. That ratio would allow for up to eight molecules of the NRP-V7/H-2K^d monomer to bind to a single CLIO particle, forming the probe designated CLIO-NRP-V7. The octomeric structure of the probe readily overcomes the low affinity of TCRs for peptide/MHC complexes; in fact, a trimeric structure is believed to be sufficient (31).

TABLE 1
Relaxation rates and mean hydrodynamic diameter of the conjugates

	CLIO-NH_2	CLIO-avidin	CLIO-NRP
R1 (mmol · l^{-1} · s^{-1})	22.54	29.98	33.87
R2 (mmol · l^{-1} · s^{-1})	43.69	81.8	98.61
Size (nm)	29.5	68.8	114.1

To further confirm the synthesis of CLIO-avidin and to assess its ability to react with high-molecular biotinylated proteins, we measured the changes in the spin-spin relaxation time (T2) that occurred upon binding with multibiotinylated BSA and thus confirmed reactivity (29). Magnetic properties and mean hydrodynamic diameter of the conjugates determined by laser light scattering are presented in Table 1. Upon conjugation to avidin and subsequently to the NRP-V7/H-2K^d monomer, the sizes of the conjugates were 68.8 nm for CLIO-avidin and 114.1 nm for CLIO-NRP-V7.

The CLIO-NRP-V7 probe is specific for NRP-V7–reactive $CD8^+$ T-cells both in vitro and in vivo. The specificity of the CLIO-NRP-V7 probe was tested by flow cytometry as well as in cell-binding assays using $CD8^+$ T-cells derived from wild-type NOD mice or NOD mice expressing a transgenic NRP-V7–reactive TCR (23,24) (8.3-NOD mice). Whereas the CLIO-NRP-V7 probe labeled almost all 8.3-NOD–derived $CD8^+$ T-cells (92%; Fig. 2*A*), it labeled only 1.86% of NOD-derived $CD8^+$ cells (Fig. 2*B*). This demonstrated that the CLIO-NRP-V7 probe has a high degree of specificity for NRP-V7–reactive $CD8^+$ T-cells.

Because it would be clinically relevant to be able to administer the probe systemically to label autoreactive $CD8^+$ T-cells, we investigated whether labeling of NRP-V7–reactive $CD8^+$ T-cells could be accomplished by systemic administration of the CLIO-NRP-V7 probe to 8.3-NOD mice. Approximately 90% of peripheral blood $CD8^+$ T-cells from CLIO-NRP-V7–injected 8.3-NOD mice were positive on the FL1 channel (FITC label on avidin), indicating that they had bound CLIO-NRP-V7 (Fig. 2*C*). Similar results (92%) were obtained with 8.3-$CD8^+$ T-cells stained with soluble NRP-V7/H-2K^d tetramers (data not shown). These results demonstrate that conjugation of the peptide-MHC complex to CLIO-avidin did not compromise its avidity for $CD8^+$ T-cells. In contrast, only ~2% of the peripheral blood $CD8^+$ T-cells of pre-diabetic NOD mice were FITC positive. These results are similar to those obtained by labeling $CD8^+$ T-cells ex vivo (see above). It is noteworthy that CLIO-NRP-V7 stained a slightly higher percentage of $CD8^+$ T-cells from wild-type NOD mice than soluble NRP-V7/H-2K^d tetramers (0.76% for 12-week-old NOD mouse [25]). Because $CD8^+$ T-cells that recognize NRP-V7 with very low avidity do not bind efficiently to NRP-V7/H-2K^d tetramers (B. Han and P. Santamaria, unpublished observations) and because the CLIO-NRP-V7

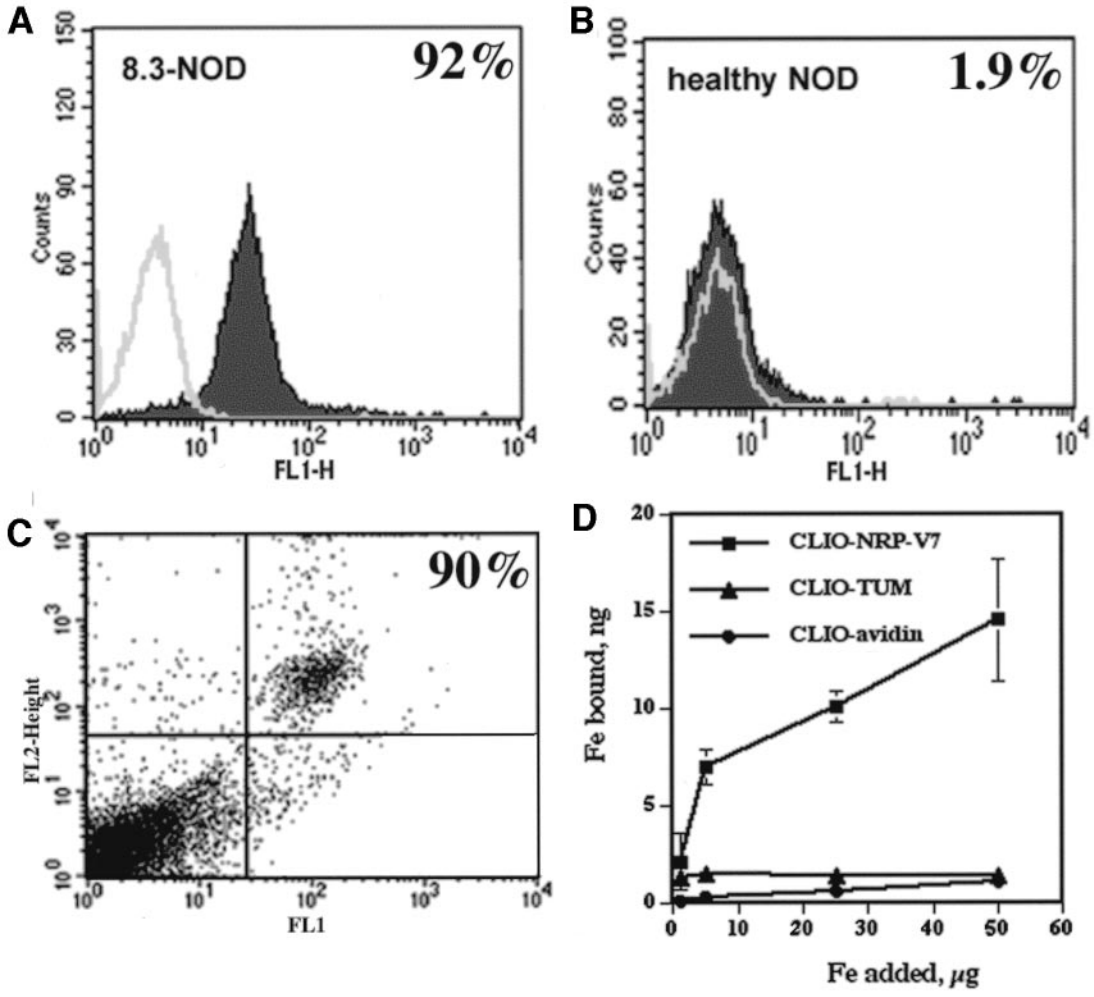

FIG. 2. FACS analysis of CD8+ cells incubated with immunomagnetic probe CLIO-NRP-V7: *A*: CD8+ T-cells from nondiabetic 8.3-NOD mice. *B*: CD8+ cells from nondiabetic wild-type NOD mice. *C*: FACS analysis of the cells from the whole blood of 8.3-NOD mice that received an injection of CLIO-NRP-V7. Ninety percent of CD8+ T-cells were positive for CLIO-NRP staining. *D*: Cell-binding assay: CD8+ T-cells from 8.3-NOD mice accumulated 10 times more iron from CLIO-NRP-V7 than from unmodified CLIO or irrelevant CLIO-TUM probe.

probe carries up to eight monomers (as opposed to four by the tetramers), the above differences likely are due to differences in the avidity of these two probes for NRP-V7–reactive CD8+ T-cells. In turn, this suggests that the pool of circulating NRP-V7–reactive CD8+ T-cells in wild-type NOD mice is higher than previously thought (25).

Fluorescence microscopy studies on labeled cells demonstrated that the CLIO-NRP-V7 probe was predominantly located inside the cells, presumably resulting from internalization of TCR/CLIO-NRP-V7 complexes (32). Internalization of the probe by these T-cells was specific, because virtually no uptake was observed with an unmodified CLIO-avidin probe or with irrelevant CLIO-TUM conjugate (Fig. 2*D*).

Cytotoxicity assays demonstrated that the probe was not toxic to labeled cells. Furthermore, labeled and unlabeled 8.3-CD8+ T-cells cells produced comparable levels of interleukin-2 and interferon-γ (Fig. 3*A*) and differentiated equally well into cytotoxic effectors in response to NRP-V7–pulsed, irradiated NOD splenocytes as antigen-

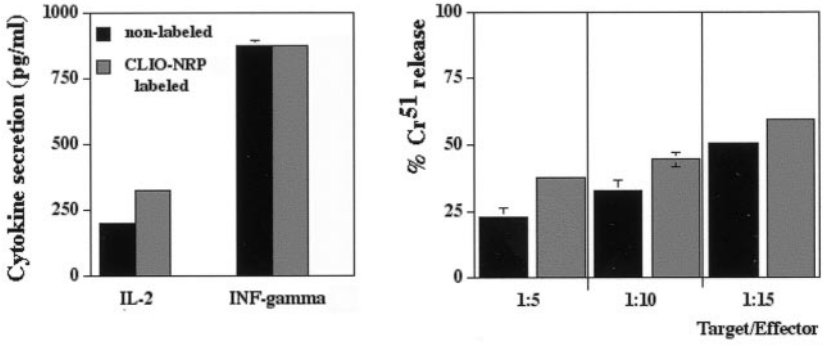

FIG. 3. Labeling with CLIO-NRP-V7 did not affect cytokine secretion of labeled CD8+ T-cells (*left*) or their ability to differentiate into cytolytic effectors in vitro (*right*). Data correspond to average ± SD of duplicate (*left*) or triplicate (*right*) cultures.

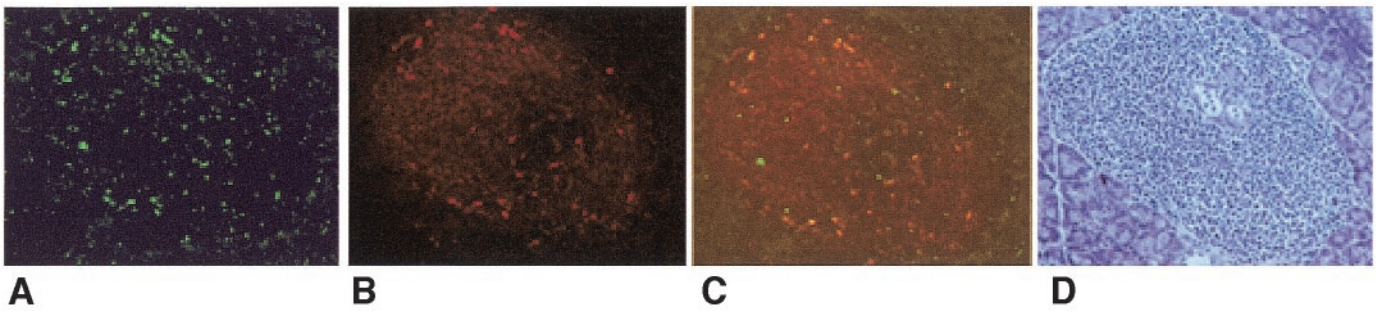

FIG. 4. Dual-channel fluorescence microscopy of the frozen pancreatic section from 8.3-NOD mice after incubation with CLIO-NRP-V7 (*A*; green channel) and anti–CD8-PE (*B*; red channel). Combination image shows colocalization of two signals (*C*). *D*: H&E stain of the same islet on the consecutive section confirmed the presence of infiltrating mononuclear cells in the islet. Magnification ×20.

presenting cells (Fig. 3*B*). To ascertain whether the CLIO-NRP-V7 probe could also detect islet-associated $CD8^+$ T-cells in situ, we investigated the ability of CLIO-NRP-V7 to stain islet-associated $CD8^+$ T-cells in pancreas sections from acutely diabetic 8.3-NOD mice. Figure 4 shows representative images of islets stained with CLIO-NRP-V7 (Fig. 4*A*, green channel), anti–CD8-PE (Fig. 4*B*, red channel), and the combination image (Fig. 4*C*), demonstrating colocalization of two signals. H&E staining (Fig. 4*D*) of immediately adjacent sections confirmed the presence of mononuclear cells in these islets. It should be noted that a number of all islet-associated lymphocytes (*panel D*, H&E stain) do not seem to be fluorescent in *panels A–C* because a considerable number of islet-associated cells in 8.3-NOD mice are not $CD8^+$ but rather $CD4^+$ (approximately one-third). Also, macrophages as well as a significant number of B-cells that are not labeled with CLIO-NRP-V7 or anti-CD8 antibody are present in the islets of 8.3-NOD mice. These results demonstrate that CLIO-NRP-V7 is also a useful probe to detect the presence of NRP-V7–reactive $CD8^+$ T-cells in tissue sections.

In vivo MRI of $CD8^+$ T-cell infiltration. We next sought to determine whether CLIO-NRP-V7–labeled 8.3-$CD8^+$ T-cells were amenable to in vivo MRI studies. $CD8^+$ T-cells from 8.3-NOD mice were labeled with CLIO-NRP-V7 and then adoptively transferred into 5-week-old NOD.scid mice. Figure 5*A* shows representative images of the pancreas on the day of cell transfer and 9 days later. Darkening of the pancreatic tissue on the T2-weighted images results from accumulation of magnetically labeled cells. The tissue became darker over time as more labeled cells accumulated in the pancreas. Color-coded images (Fig. 5*B*) demonstrate that darkening of the T2-weighted images corresponds to a decrease in SI from high (yellow) to low (red). It is important to note here that no changes were observed in the spleen, liver, or muscle tissue of the same mice, and no changes were noticed after the transfer of unlabeled cells, indicating that CLIO-NRP-V7 SI labeled cells predominantly (if not exclusively) accumulated in the pancreas, as expected. Although T-cells undergo homeostatic expansion upon transfer into immunodeficient hosts, it is highly unlikely that recruitment of the transferred T-cells to the pancreas was due to this. We have previously shown that in recombination-activating gene-2 SI– deficient TCR-transgenic NOD mice (mice that can exclusively export $CD8^+$ T-cells expressing the transgenic TCR), naïve 8.3-$CD8^+$ T-cells spontaneously travel to pancreatic islets but not to any other tissue (21). In any case, the data show that T-cell proliferation in the hosts did not significantly affect probe SI below the threshold of detection (owing to cell division) for at least 16 days after transfer.

Comparison of the SI in the pancreas and external control allowed an assessment of T-cell accumulation in the pancreas as a function of time. Changes in SI in the pancreas were noted as early as 2 days after T-cell transfer and continued up to day 16 (Fig. 5*C*). The blood glucose levels in the mice remained unchanged throughout the course of the study. Fluorescence microscopy of pancreatic sections from these mice revealed the presence of FITC-positive $CD8^+$ T-cells (Fig. 5*D*). Histological H&E stain of the consecutive sections confirmed the infiltration of transferred lymphocytes in the islets.

DISCUSSION

Using $CD8^+$ T-cells derived from a transgenic NOD mouse expressing a representative, highly diabetogenic TCR as a model, we have shown that it is possible to visualize the recruitment of autoreactive T-cells to the pancreas in real time using high-resolution MRI. This was accomplished by labeling T-cells with a novel, antigen-specific magnetic label. This label, which is based on superparamagnetic nanoparticles coated with peptide/MHC monomers, is specifically recognized by the TCRs of a prevalent population of autoreactive $CD8^+$ T-cells that play an important role in the natural history of diabetes in NOD mice. Upon binding, the probe is endocytosed by the T-cells, such that accumulation of these T-cells in the pancreas can be visualized by high-resolution MRI.

Notably, the probe labeled a significant percentage of peripheral blood $CD8^+$ T-cells from wild-type NOD mice, both in vivo after systemic administration of the probe and ex vivo, upon incubation of $CD8^+$ T-cells with the label in vitro. The ability of CLIO-NRP-V7 to label the circulating NRP-V7–reactive $CD8^+$ T-cell pool is not unexpected. We have previously shown that the cumulative percentage of NRP-V7–reactive $CD8^+$ T-cells in peripheral blood is a highly sensitive and specific predictor of diabetes progression in NOD mice (25). The fact that CLIO-NRP-V7 can be used to label the circulating NRP-V7–reactive $CD8^+$ T-cells of wild-type NOD mice is important because it shows that our strategy might be applicable to humans, if equivalent subpopulations of human autoreactive $CD8^+$ T-cells are

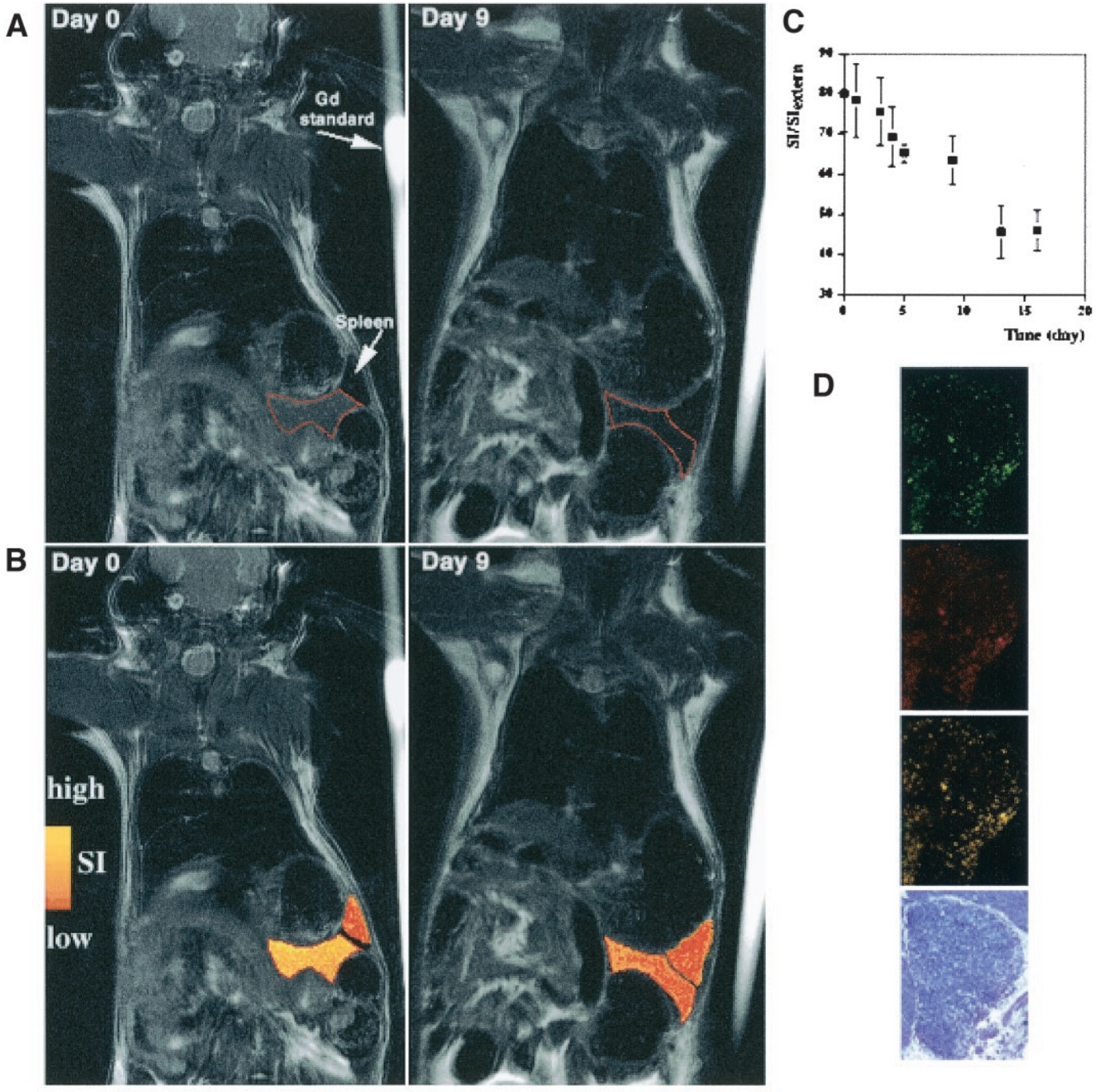

FIG. 5. *A*: **In vivo imaging of pancreatic infiltration of CD8$^+$ T-cell labeled with CLIO-NRP-V7 and adoptively transferred into 5-week-old NOD.scid mice.** *B*: **Color-encoded SI of the spleen and the tail of the pancreas.** *C*: **The decrease of SI from day 0 to day 16 in the pancreas (outlined in red) is due to the accumulation of CLIO-NRP-V7–labeled CD8$^+$ T cells.** *D*: **Dual-channel fluorescence microscopy of the excised pancreas after the 16th day of MRI. Green channel shows the presence of CLIO-NRP-V7–labeled cells in the islet; staining with anti–CD8-PE antibodies (red channel) confirmed the presence of transferred cells. Superimposition of two images shows that CLIO-NRP-V7–labeled cells were also positive for CD8$^+$ T-cell marker. Histological H&E stain of the same islet (consecutive section) shows the infiltration of mononuclear cells in the islet. Magnification ×20.**

identified. The naturally occurring ligand of the NRP-V7–reactive CD8$^+$ T-cell subset has been recently identified. It corresponds to a nonamer peptide derived from islet-specific glucose-6-phosphatase catalytic subunit–related protein (IGRP) (33). It is noteworthy that this autoantigen is also expressed in human islets and that it is encoded in a locus that is linked to a diabetes-associated type 1 diabetes gene (34). Because IGRP $_{206–214}$/H-2K^d and NRP-V7/H-2K^d tetramers stain similar percentages of circulating and islet-associated CD8$^+$ T-cells (33), imaging probes using IGRP$_{206–214}$/H-2K^d monomers would be expected to work equally well. If IGRP-reactive CD8$^+$ T-cells were also prevalent in the circulation of human pre-diabetic individuals, then similar probes could be used to visualize and therefore diagnose the presence of islet inflammation. In this regard, it should be emphasized that labeling of

NRP-V7–reactive $CD8^+$ T cells with CLIO-NRP-V7 at levels that can be detected in vivo by MRI is not cytotoxic to the labeled cells and does not seem to elicit their diabetogenic activity.

Previous studies on lymphocyte tracking using MRI (35,36) relied on labeling the total lymphocyte pool with magnetic probes. Alternatively, an optical imaging method for monitoring the autoimmune process in transplanted islets was introduced recently (37). Here we have shown that it is possible to image selectively the accumulation of T-cells of defined antigenic reactivity. We observed a change of SI on MR images for up to 16 days after the transfer of labeled cells. This change resulted from progressive accumulation of labeled $CD8^+$ T-cells in the pancreas. We have to emphasize that the distribution of the labeled cells within the pancreas seems to follow a heterogeneous pattern, presumably as a result of the difference in islet density throughout the pancreas.

We have noted that cell division results in equal redistribution of the probe between parent and daughter cells (A.M., unpublished data). Therefore, it is possible that in situ proliferation of accumulated cells may cause "signal dilution" as a result of label redistribution between dividing cells. However, it is compensated by enhancement of the signal owing to progressive recruitment and accumulation of labeled cells within the tissue. The rate of this phenomenon and the detection threshold of the proliferated labeled cells is a subject of a separate investigation currently under study in our laboratory. Also, we anticipate that the natural insensitivity of MRI can be overcome by using robust amplification techniques based on cellular internalization of superparamagnetic probes such as the cross-linked iron oxide nanoparticles used in this study.

To the best of our knowledge, this study represents the first demonstration of detection of an autoimmune response by MRI in live animals. Our strategy has the potential to allow the visualization of prevalent populations of autoreactive T-cells in humans noninvasively. This approach potentially could be used to monitor the outcome of therapeutic intervention, including pancreas and islet transplantation.

ACKNOWLEDGMENTS

This work was supported in part by grants from the American Diabetes Association (Junior Faculty Award to A.M.), the National Institutes of Health (RO1 DK63572 and RO1 DK064850 to A.M.), the Juvenile Diabetes Research Foundation (to A.M.), and the Canadian Institutes of Health Research (to P.S.). J.G. is a recipient of a fellowship from the German Research Society (Deutsche Forschungsgemeinschaft). P.S. is a scientist of the Alberta Heritage Foundation for Medical Research.

We thank Dr. Nikolay Sergeyev for CLIO synthesis and Drs. Lee Josephson, Ralph Weissleder, and Jennifer Allport for helpful suggestions.

REFERENCES

1. Liblau R, Wong S, Mars L, Santamaria P: Autoreactive CD8+ T-cells in organ-specific autoimmunity: emerging targets for therapeutic intervention. *Immunity* 17:1–6, 2002
2. Weissleder R: Molecular imaging: exploring the next frontier. *Radiology* 212:609–614, 1999
3. Oku N, Koike C, Sugawara M, Tsukada H, Irimura T, Okada S: Positron emission tomography analysis of metastatic tumor cell trafficking. *Cancer Res* 54:2573–2576, 1994
4. Koike C, Watanabe M, Oku N, Tsukada H, Irimura T, Okada S: Tumor cells with organ-specific metastatic ability show distinctive trafficking in vivo: analyses by positron emission tomography and bioimaging. *Cancer Res* 57:3612–3619, 1997
5. Kikkawa H, Tsukada H, Oku N: Usefulness of positron emission tomographic visualization for examination of in vivo susceptibility to metastasis. *Cancer* 89:1626–1633, 2000
6. Melder R, Munn L, Stoll B, Marecos E, Baxter L, Weissleder R, Jain R: Systemic distribution and tumor localization of adoptively transferred lymphocytes in mice: comparison with physiologically based pharmacokinetic model. *Neoplasia* 4:3–8, 2002
7. Adonai N, Nguyen KN, Walsh J, Iyer M, Toyokuni T, Phelps ME, McCarthy T, McCarthy DW, Gambhir SS: Ex vivo cell labeling with 64Cu-pyruvaldehyde-bis(N4-methylthiosemicarbazone) for imaging cell trafficking in mice with positron-emission tomography. *Proc Natl Acad Sci U S A* 99:3030–3035, 2002
8. Hardy J, Edinger M, Bachmann M, Negrin RS, Fathman CG, Contag CH: Bioluminescence imaging of lymphocyte trafficking in vivo. *Exp Hematol* 29:1353–1360, 2001
9. Costa GL, Sandora MR, Nakajima A, Nguyen EV, Taylor-Edwards C, Slavin AJ, Contag CH, Fathman CG, Benson JM: Adoptive immunotherapy of experimental autoimmune encephalomyelitis via T cell delivery of the IL-12 p40 subunit. *J Immunol* 167:2379–2387, 2001
10. Bhaumik S, Gambhir S: Optical imaging of Renilla luciferase reporter gene expression in living mice. *Proc Natl Acad Sci U S A* 99:377–382, 2002
11. Scheffold C, Kornacker M, Scheffold Y, Contag C, Negrin R: Visualization of effective tumor targeting by CD8+ natural killer T cells redirected with bispecific antibody F(ab′)(2)HER2xCD3. *Cancer Res* 62:5785–5791, 2002
12. Edinger M, Cao Y, Verneris M, Bachmann MH, Contag CH, Negrin RS: Revealing lymphoma growth and the efficacy of immune cell therapies using in vivo bioluminescence imaging. *Blood* 101:640–648, 2003
13. Jain R, Munn L, Fukumura D: Dissecting tumour pathophysiology using intravital microscopy. *Nat Rev Cancer* 2:266–276, 2000
14. Moore A, Weissleder R, Bodganov A: Uptake of dextran-coated monocrystalline iron oxides in tumor cells and macrophages. *J Magn Reson Imaging* 7:1140–1145, 1997
15. Weissleder R, Cheng H, Bogdanova A, Bogdanov AJ: Magnetically labeled cells can be detected by MR imaging. *J Magn Reson Imaging* 7:258–263, 1997
16. Lewin M, Carlesso N, Tung C, Tang X, Cory D, Scadden D, Weissleder R: Tat peptide-derivatized magnetic nanoparticles allow in vivo tracking and recovery of progenitor cells. *Nat Biotechnol* 18:410–414, 2000
17. Dodd C, Hsu H, Chu W, Yang P, Zhang H, Mountz J Jr, Zinn K, Forder J, Josephson L, Weissleder R, Mountz J, Mountz J: Normal T-cell response and in vivo magnetic resonance imaging of T-cells loaded with HIV transactivator-peptide-derived superparamagnetic nanoparticles. *J Immunol Methods* 256:89–105, 2001
18. Moore A, Sun P, Cory D, Högemann D, Weissleder R, Lipes M: MRI of insulitis in autoimmune diabetes. *Magn Reson Med* 47:751–758, 2002
19. Santamaria P, Utsugi T, Park B, Averill N, Kawazu S, Yoon J: Beta cell cytotoxic CD8+ T cells from non-obese diabetic mice use highly homologous T cell receptor alpha chain CDR3 sequences. *J Immunol* 154:2494–2503, 1995
20. Verdaguer J, Yoon J, Anderson B, Averill N, Utsugi T, Park BJ, Santamaria P: Acceleration of spontaneous diabetes in TCRb-transgenic nonobese diabetic mice by beta cell-cytotoxic CD8+ T-cells expressing identical endogenous TCRa chains. *J Immunol* 157:4726–4735, 1996
21. Verdaguer J, Schmidt D, Amrani A, Anderson B, Averill N, Santamaria P: Spontaneous autoimmune diabetes in monoclonal T cell nonobese diabetic mice. *J Exp Med* 186:1663–1676, 1997
22. DiLorenzo T, Graser T, Ono T, Christianson G, Chapman H, Roopenian D, Nathenson S, Serreze D: MHC class I-restricted T-cells are required for all but end stages of diabetes development and utilize a prevalent T cell receptor a chain gene rearrangement. *Proc Natl Acad Sci U S A* 95:12538–12543, 1998
23. Anderson B, Park B, Verdaguer J, Amrani A, Santamaria P: Prevalent CD8+ T cell response against one peptide/MHC complex in autoimmune diabetes. *Proc Natl Acad Sci U S A* 96:9311–9316, 1999
24. Amrani A, Serra P, Yamanouchi J, Trudeau J, Tan R, Elliott J, Santamaria P: Expansion of the antigenic repertoire of a single T cell receptor upon T cell activation. *J Immunol* 167:655 666, 2001
25. Trudeau J, Kelly-Smith C, Verchere B, Finegood D, Santamaria P, Tan R: Autoreactive T cells in peripheral blood predict development of type 1 diabetes. *J Clin Invest* 111:217–223, 2003
26. Amrani A, Verdaguer J, Serra P, Tafuro S, Tan R, Santamaria P: Progression of autoimmune diabetes driven by avidity maturation of a T-cell population. *Nature* 406:739–742, 2000

27. Josephson L, Tung C, Moore A, Weissleder R: High-efficiency intracellular magnetic labeling with novel superparamagnetic-Tat peptide conjugates. *Bioconjug Chem* 10:186–191, 1999
28. Shen T, Weissleder R, Papisov M, Bogdanov A, Brady T: Monocrystalline iron oxide nanocompounds (MION): physicochemical properties. *Magn Reson Med* 29:599–604, 1993
29. Perez J, Josephson L, O'Loughin T, Högemann D, Weissleder R: Magnetic relaxation switches capable of sensing molecular interaction. *Nat Biotechnol* 20:816–820, 2002
30. Ljunggren H, Stam N, Öhlden C, Neefjes J, Hoglund P, Heemels M, Bastin J, Schumacher T, Townsend A, Karre K: Empty MHC class I molecules come out in the cold. *Nature* 346:476–480, 1990
31. Davis M, Boniface J, Reich Z, Lyons D, Hampl J, Arden B, Chien Y: Ligand recognition by alpha-beta T cell receptors. *Annu Rev Immunol* 16:523–544, 1998
32. Liu H, Rhodes M, Wiest D, Vignali D: On the dynamic of TCR:CD3 complex cell surface expression and downmodulation. *Immunity* 13:665–675, 2000
33. Lieberman S, Evans A, Han B, Takaki T, Vinnitskaya Y, Caldwell JA, Serreze DV, Shabanowitz J, Hunt DF, Nathenson SG, Santamaria P, DiLorenzo TP: Identification of the b-cell antigen targeted by a prevalent population of pathogenic CD8+ T cells in autoimmune diabetes. *Proc Natl Acad Sci U S A* 100:8384–8388, 2003
34. Owerbach D: Physical and genetic mapping of IDDM8 on chromosome 6q27. *Diabetes* 49:508–512, 2000
35. Yeh T, Zhang W, Ildstad S, Ho C: Intracellular labeling of T-cells with superparamagnetic contrast agents. *Magn Reson Med* 30:617–625, 1993
36. Yeh T, Zhang W, Ildstad S, Ho C: In vivo dynamic MRI tracking of rat T-cells labeled with superparamagnetic iron-oxide particles. *Magn Reson Med* 33:200–208, 1995
37. Bertera S, Geng X, Tawadrous Z, Bottino R, Balamurugan AN, Rudert WA, Drain P, Watkins SC, Trucco M: Body window-enabled in vivo multicolor imaging of transplanted mouse islets expressing an insulin-timer fusion protein. *Biotechniques* 35:718–722, 2003